The Conformations of a Substrate and a Product Bound to the Active Site of *S*-Adenosylmethionine Synthetase†

Céline Schalk-Hihi‡ and George D. Markham*

Institute for Cancer Research, Fox Chase Cancer Center, 7701 Burholme Avenue, Philadelphia, Pennsylvania 19111

Received September 23, 1998; Revised Manuscript Received December 21, 1998

ABSTRACT: *S*-Adenosylmethionine (AdoMet) is the most widely used alkyl group donor in biological systems. The formation of AdoMet from ATP and L-methionine is catalyzed by *S*-adenosylmethionine synthetase (AdoMet synthetase). Elucidation of the conformations of enzyme-bound substrates, product, and inhibitors is important for the understanding of the catalytic mechanism of the enzyme and the design of new inhibitors. To obtain structural data for enzyme-bound substrates and product, we have used two-dimensional transferred nuclear Overhauser effect spectroscopy to determine the conformation of enzyme-bound AdoMet and 5′-adenylyl imidodiphosphate (AMPPNP). AMPPNP, an analogue of ATP, is resistant to the ATP hydrolysis activity of AdoMet synthetase because of the presence of a nonhydrolyzable NH-link between the β- and γ-phosphates but is a substrate for AdoMet formation during which tripolyphosphate is produced. AdoMet and AMPPNP both bind in an *anti* conformation about the glycosidic bond. The ribose rings are in $C_{3'}$-*exo* and $C_{4'}$-*exo* conformations in AdoMet and AMPPNP, respectively. The differences in ribose ring conformations presumably reflect the different steric requirements of the C5′ substituents in AMPPNP and AdoMet. The NMR-determined conformations of AdoMet and AMPPNP were docked into the *E. coli* AdoMet synthetase active site taken from the enzyme·ADP·P_i crystal structure. Since there are no nonexchangeable protons either in the carboxy-terminal end of the methionine segment of AdoMet or in the tripolyphosphate segment of AMPPNP, these portions of the molecules were modeled into the enzyme active site. The interactions of AdoMet and AMPPNP with the enzyme predict the location of the methionine binding site and suggest how the positive charge formed on the sulfur during AdoMet synthesis is stabilized.

S-Adenosylmethionine (AdoMet)[1] is the primary alkylating agent in biological systems (*1*, *2*). AdoMet is a methyl donor in the methylation of DNA, RNA, and proteins and alternatively undergoes decarboxylation to generate the propylamine donor used in spermine and spermidine biosynthesis (*1*, *2*). The metabolic importance of AdoMet has resulted in numerous attempts to obtain potent inhibitors of its synthesis (*3*, *4*); however, these studies have not benefited from three-dimensional structural information. The formation of AdoMet is catalyzed by *S*-adenosylmethionine synthetase (AdoMet synthetase, EC 2.5.1.6, ATP:L-methionine *S*-adenosyltransferase) in a two-step reaction from ATP and L-methionine (*5*). First, AdoMet is formed by direct attack of the sulfur atom of methionine on the C5′ atom of ATP in an S_N2 reaction, with cleavage of the complete tripolyphosphate chain from ATP. In the second reaction, the tripolyphosphate is asymmetrically hydrolyzed to PP_i and P_i before any products are released. Two divalent metal ions such as Mg^{2+} bind to the enzyme active site in the presence of ATP, or an analogue thereof, and are both required for activity (*6*−*8*); a single divalent cation binds in the presence of AdoMet. K^+, or another monovalent cation of equivalent size, stimulates the rate of AdoMet formation up to 100-fold (*9*). Sequence homologies among AdoMet synthetase from various sources show that AdoMet synthetase is an exceptionally well-conserved enzyme within eukarya and prokarya. In particular, residues present in the active site are all conserved in each of the reported AdoMet synthetase sequences (*10*−*19*).

The crystal structure of *E. coli metK*-encoded AdoMet synthetase isozyme has been solved at 3 Å resolution (*20*). The enzyme consists of 4 identical 383 residue subunits. Each subunit consists of three structural domains related to each other by a pseudo-3-fold symmetry. Pairs of subunits interact with each other to form tight dimers. Each dimer contains two active sites located between the subunits. The divalent and monovalent metal binding sites (K^+ and Mg^{2+}) lie in a large, deep active site cleft. The crystal structures of AdoMet synthetase in complexes formed with the substrates ATP and 8-Br-ATP and the product PP_i were also studied (*21*). In the crystals, the triphosphates were hydrolyzed to diphosphates and P_i by the enzyme's intrinsic ATPase activity. ADP (8-Br-ADP) and P_i were found in the active site along with the essential metal ions K^+ and Mg^{2+}, revealing some aspects of their binding modes. However, the conformation of the adenosyl moiety was not well-defined due to disorder of the

† This work was supported by National Institutes of Health Grants GM31186 and CA06927, and was also supported by an appropriation from the Commonwealth of Pennsylvania.

* To whom correspondence should be addressed. Telephone: 215-728-2439. Fax: 215-728-3574. E-mail: GD_Markham@fccc.edu.

‡ Present address: 3D Pharmaceuticals Inc., Exton, PA.

[1] Abbreviations: AdoMet, *S*-adenosylmethionine; AMPPNP, 5′-adenylyl imidodiphosphate; AdoMet synthetase, *S*-adenosylmethionine synthetase; P_i, orthophosphate; PP_i, pyrophosphate; NOE, nuclear Overhauser effect; TRNOE, transferred nuclear Overhauser effect; TRNOESY, transferred nuclear Overhauser effect spectroscopy; FID, free induction decay; TPPI, time-proportional phase incrementation.

10.1021/bi9822933 CCC: $18.00
Published on Web 02/05/1999

ribose group in the crystals. No information concerning the conformation and the binding mode of the product AdoMet or the nonhydrolyzable substrate AMPPNP is available, since X-ray quality crystals of these complexes have not been obtained.

Knowledge of the atomic details of a ligand−enzyme complex is important for understanding the nature of the binding interactions as well as the catalytic mechanism of enzymes. Such knowledge is also very valuable in drug design. Unfortunately, crystallographic determination of a ligand−enzyme complex structure is often a laborious process and is limited by the chances of obtaining X-ray quality crystals. In an alternative approach, two-dimensional proton transferred nuclear Overhauser effect (TRNOE) measurements allow the determination of inter-proton distances of small ligands bound to a macromolecule and have thus been widely used as an complementary method to X-ray crystallography for structural studies of ligand−protein complexes (*22*−*33*). In this study, we have used transferred nuclear Overhauser effect spectroscopy (TRNOESY) and two-dimensional ^{1}H NMR to determine the conformations of AdoMet and AMPPNP bound to the active site of the AdoMet synthetase. The computed conformations of AMPPNP and AdoMet obtained were then docked into the active site of the AdoMet synthetase crystal structure to evaluate their potential interaction with the active site residues. The structural data obtained provide insight into the catalytic mechanism and testable models for specific aspects of enzyme−substrate recognition.

EXPERIMENTAL PROCEDURES

Materials. Substrates and nondeuterated buffers were purchased from Sigma. Deuterated compounds were obtained from CDN Isotopes. 8-Deutero-ATP was prepared by exchange with D_2O at pH 10 and purified by anion exchange chromatography (*34*).

Preparation of AdoMet Synthetase from E. coli. E. coli AdoMet synthetase was purified using the procedure described elsewhere (*9*) and exchanged into perdeuterated NMR buffer (20 mM Tris-d_{11}, 1 mM dithiothreitol-d_{10}, 2% glycerol-d_8, 20 mM KCl, pD 8.1, in 99.99% D_2O) by running the protein sample through a preequilibrated PD10 column (Pharmacia). The protein was then concentrated in a Centricon PM10 concentrator to 12 mg/mL (0.29 mM active sites). Protein concentration was determined from absorbance at 280 nm using an extinction coefficient of 1.3 mg mL^{-1} cm^{-1} and a subunit molecular mass of 42 kDa (*9*).

Synthesis of (−)-AdoMet. AdoMet contains a chiral sulfonium center and can thus exist in two diastereoisomeric forms, (−)- and (+)-AdoMet. (−)-AdoMet is the only form enzymatically synthesized and is the only methyl donor in vivo. Because pure (−)-AdoMet is not commercially available, the (−)-form of AdoMet was enzymatically synthesized. The strong product inhibition was overcome by adding 8% β-mercaptoethanol to the reaction mix (*35*). Complete conversion of 10 mM ATP and 10 mM methionine into (−)-AdoMet can then be achieved. The reaction was monitored by thin-layer plate chromatography on cellulose developed in butanol·acetic acid·water (25:4:10). When the reaction was complete, the reaction mix was applied on a 16 mL Source S15 cation exchange column, preequilibrated in water. Elution of (−)-AdoMet was achieved by applying a 0−1 N HCl gradient in 150 mL. (−)-AdoMet eluted at approximately 0.7 N HCl and was lyophilized, redissolved in D_2O, and adjusted to pD 7.0. The purified (−)-AdoMet was analyzed by ^{1}H NMR in order to check its diastereoisomeric purity as the methyl group resonances of (+)- and (−)-AdoMet are well resolved.

Preparation of the AMPPNP and AdoMet NMR Samples. AMPPNP (Sigma) was subjected to three cycles of lyophilization and redissolution in 99.9% D_2O, followed by dissolution in perdeuterated NMR buffer containing 0.24 mM AdoMet synthetase active sites and 20 mM $MgCl_2$ to give a final AMPPNP concentration of 10 mM. Under these conditions, the dissociation constant for AMPPNP determined by protein fluorescence quenching was 4.5 mM. A sample containing 4 mM AMPPNP, 0.10 mM AdoMet synthetase, and 8 mM $MgCl_2$ was also studied.

Purified (−)-AdoMet was lyophilized and redissolved in perdeuterated NMR buffer, containing 0.28 mM AdoMet synthetase active sites and 20 mM $MgCl_2$ to a final concentration of 8.7 mM. The dissociation constant for (−)-AdoMet determined by fluorescence quenching was 43 μM under these conditions. A sample containing 5 mM AdoMet, 0.16 mM AdoMet synthetase, and 12 mM $MgCl_2$ was also studied.

NMR Spectroscopy. NMR spectra were recorded at 10 °C on a Bruker DMX600 NMR spectrometer. One-dimensional ^{1}H spectra were collected with a spectral width of 10 ppm by recording 32 scans after 4 dummy scans and allowing a relaxation delay of 2 s. Water suppression was achieved by selective presaturation (*36*). The NMR spectra were processed on a Silicon Graphics Indigo II computer with the program FELIX 95 (MSI, Inc.). The data were zero-filled to 8K, and a 1 Hz exponential line broadening function was applied before Fourier transformation.

Two-dimensional TRNOE spectra were collected with a spectral width of 10 ppm in both dimensions. Six data sets were collected with mixing times of 40, 70, 100, 130, 160, and 200 ms over a period of 60 h. The AdoMet synthetase was found to be fully active at the end of the experiments. For each spectrum, 500 FIDs were recorded in the TPPI mode after 64 dummy scans. For each FID, 1024 complex data points were acquired, and 32 scans were accumulated. A relaxation delay of 2 s between each scan was used. Selective presaturation was used to suppress the water peak (*36*). The two-dimensional NMR data were processed using FELIX 95. A 70°-shifted sine-square function was applied in each dimension before Fourier transformation, and the t_1 dimension was zero-filled to yield a final 1024 × 1024 matrix. The program FACELIFT (National NMR Facility in Madison, WI) was applied to the transformed matrix in order to perform base plane correction (*37*).

Nuclear Overhauser effect (NOE) cross-peak volumes were integrated and fitted as a function of mixing times to the NOE build-up equation using FELIX 95. The initial slopes of the build-up curves gave direct measurements of the cross-relaxation rates between individual proton pairs. For nucleosides, the distance between the ribose protons H1′ and H2′ ($r_{H1'-H2'}$) is 2.90 ± 0.2 Å regardless of the ribose conformation or the glycosyl torsional angle (*28*, *38*, *39*). The cross-relaxation rate between a pair of protons A and B (R_{A-B}) was, therefore, compared to the cross-relaxation rate

of the $H_{1'}-H_{2'}$ proton pair ($R_{H1'-H2'}$), and the internuclear distance between protons A and B (r_{A-B}) was calculated using eq 1.

$$r_{A-B} = r_{H1'-H2'}(R_{H1'-H2'}/R_{A-B})^{1/6} \quad (1)$$

One-dimensional TRNOE experiments used to study the binding specificity of AMPPNP and AdoMet were performed by using the double pulse field gradients spin−echo (DPFGSE) sequence, which eliminates "subtraction artifacts" which arise in classical NOE difference experiments from incomplete subtraction between the irradiated and control spectra (*40*−*42*). The AMPPNP and AdoMet H1′ ribose protons were selectively preirradiated. The nonselective 90° pulse was followed by a DPFGSE sequence with selective 90° and 180° pulses of duration 25 and 50 ms, respectively, shaped to a 11% truncated Gaussian. The gradients used were of 1 ms duration with a 500 μs delay for gradient recovery. For each spectrum, 1024 FIDs were recorded without dummy scans over a spectral width of 10 ppm. A relaxation delay of 2 s was used, and the measurements were done at a mixing time of 120 ms. Prior to Fourier transformation, the free induction decays were multiplied by a 1 Hz exponential line broadening function. The magnitude of the NOE was determined from peak heights.

Model Building and Energy Minimization. A constrained energy minimization protocol was carried out using the program MacroModel (version 5.5, Department of Chemistry, Columbia University), with the AMBER* force field (implicitly in vacuo). The interproton distances determined from the TRNOE experiment were used as constraints, allowing a 10% uncertainty in distances without energy penalty. For both AMPPNP and AdoMet, a Monte Carlo method was used to generate 2000 starting conformations, which were then subjected to constrained minimization. No constraints were applied to the carboxy-terminal end of the methionine segment of AdoMet for which no NOE-derived distances were available. For AMPPNP, constraints were only applied to the adenosyl portion. Ranges of conformations consistent with the NOE constraints were determined from the variation in structures that emerged from this procedure.

Docking of the AMPPNP and AdoMet NMR Structures with AdoMet Synthetase. The NOE-derived computed conformations of AMPPNP and AdoMet were docked into the *E. coli* AdoMet synthetase active site using the program CHAIN (*43*). The crystal structure used was that of AdoMet synthetase in a complex with ADP and P_i (*21*). Coordinates were obtained from the Brookhaven Protein Data Bank (File 1mxb). The search for a favorable docked conformation of AMPPNP and AdoMet was carried out in two stages. Initially, the adenine rings of AMPPNP and AdoMet were superimposed with the reference coordinate set of the adenine ring of ADP, using the crystal structure of AdoMet synthetase and the NOE-derived conformations of AMPPNP and AdoMet as rigid objects. The PPNP moiety of AMPPNP and the α-carbon substituents of AdoMet, for which nonexchangeable protons are not present and thus no structural information was available, were then manually reoriented to optimize hydrogen bonds with the enzyme active site residues and interactions with the two Mg^{2+} ions. For AMPPNP, the α-phosphate and γ-phosphate groups were manually superimposed with the α-phosphate of ADP and free P_i, respectively.

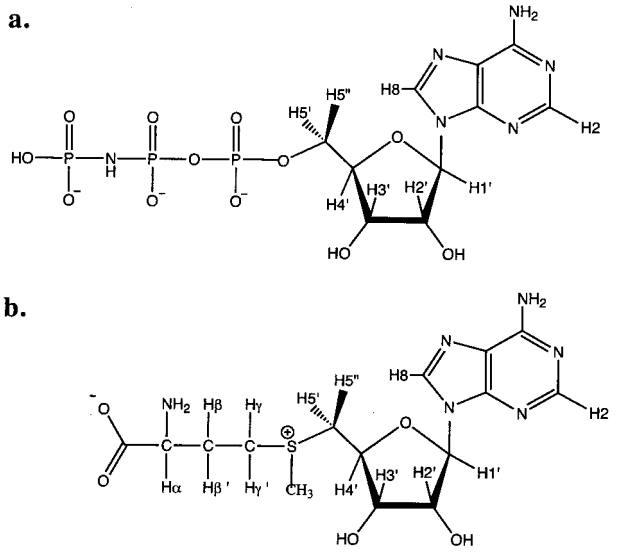

FIGURE 1: Schematic representation and numbering system of (a) AMPPNP and (b) AdoMet.

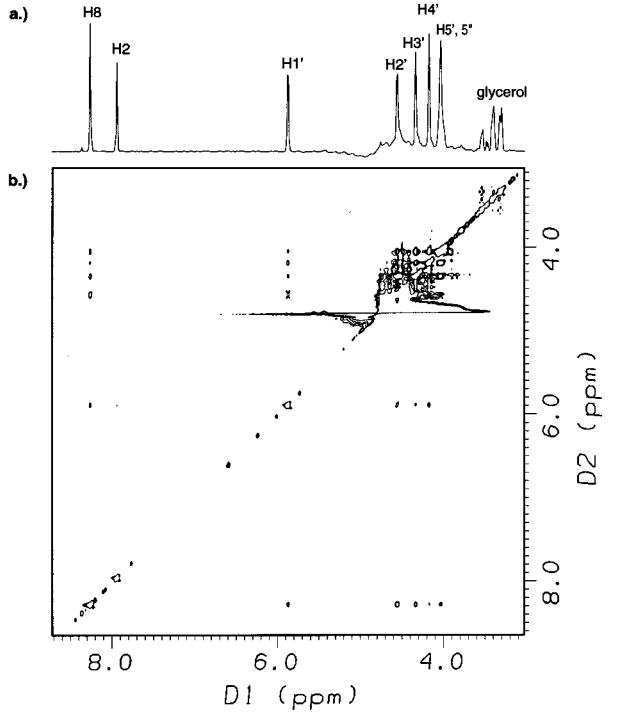

FIGURE 2: (a) One-dimensional 600 MHz ^{1}H NMR spectrum of the AdoMet synthetase (0.24 mM active sites), 10 mM AMPPNP, 20 mM $MgCl_2$ mixture in 99.99% D_2O containing 20 mM Tris-d_{11}, 1 mM dithiothreitol-d_{10}, 2% glycerol-d_8, 20 mM KCl, pD 8.1 at 10 °C; (b) NOESY spectrum of the same sample obtained at 200 ms mixing time.

RESULTS AND DISCUSSION

1D ^{1}H Spectrum of AMPPNP and (−)-AdoMet and Chemical Shift Assignments. The numbering of the various protons of AMPPNP and (−)-AdoMet is shown in Figure 1. The ^{1}H resonances of AMPPNP were assigned based on previously published chemical shifts (see Figure 2) (*44*). The assignment of the (−)-AdoMet ^{1}H resonances was in part based on published incomplete chemical shifts (*45*, *46*) which

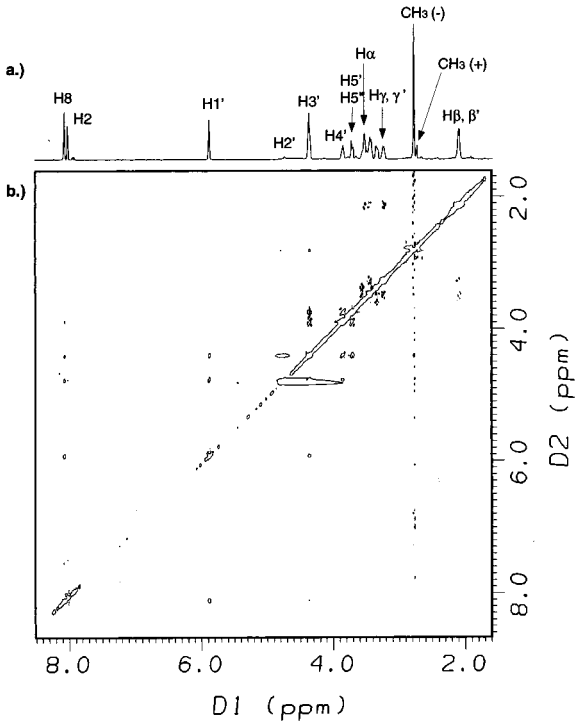

FIGURE 3: (a) One-dimensional 600 MHz ^{1}H NMR spectrum of the AdoMet synthetase (0.28 mM active sites), 8.7 mM AdoMet, 20 mM $MgCl_2$ mixture in 99.99% D_2O containing 20 mM Tris-d_{11}, 1 mM dithiothreitol-d_{10}, 2% glycerol-d_8, 20 mM KCl, pD 8.1 at 10 °C; the H2′ signal is partially suppressed due to proximity to the HDO resonance that was presaturated. (b) NOESY spectrum of the same sample obtained at 200 ms mixing time.

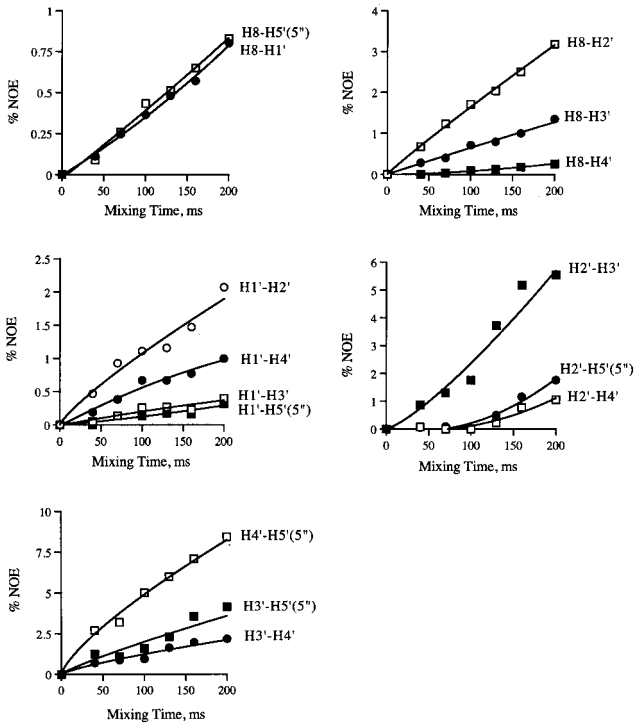

FIGURE 4: NOE intensity build-up curves for the NOE cross-peaks of different proton pairs of AdoMet synthetase-bound AMPPNP. The relative NOE intensity of each proton pair was measured as the ratio of the peak volume at different mixing times to the volume of the H1′ diagonal peak at zero mixing time. The volume at zero mixing time of the H1′ diagonal peak was determined by extrapolating the linear increase in peak volume with decreasing mixing times to zero mixing time.

were completed and confirmed with a COSY spectrum. Protons H8 and H2 as well as the ribose proton H1′ were well-resolved with chemical shifts of 8.08, 8.03, and 5.89 ppm, respectively (Figure 3a). The assignments of the H8 and H2 protons were confirmed in a spectrum of 8-deutero-(−)-AdoMet synthesized from 8-deutero-ATP and L-methionine. The ribose protons H2′, H3′, H4′, and H5′ (5″) gave multiple peaks at 4.79, 4.39, 3.88, and 3.73 ppm, respectively. A resonance for the Hα proton of the AdoMet methionine side chain was observed at 3.45 ppm. The Hγ-(γ') protons, which are not equivalent, gave multiple peaks at 3.36 ppm. The methionine Hβ(β') protons had a chemical shift of 2.11 ppm. The methylsulfonium protons of (−)- and (+)-AdoMet can be easily distinguished by ^{1}H NMR (*45*, *46*). The (−)-AdoMet which was used for the TRNOE experiments showed a major peak from (−)-AdoMet at 2.79 ppm and a peak at 2.74 ppm with ∼10% of the area of the peak at 2.79 ppm, indicating that a low level of spontaneous epimerization occurred during preparation (*47*). However, the 10:1 ratio of (−)-AdoMet to (+)-AdoMet did not evolve further over the time of the NMR experiment. No attempts were made to further purify (−)-AdoMet from (+)-AdoMet.

Time-Dependent TRNOE of AMPPNP and AdoMet. Nonspecific binding of a ligand to an enzyme might make a contribution to observed TRNOEs and the TRNOE-derived distances, thus leading to a ligand conformation which reflects an average conformation between specifically and nonspecifically bound ligand (*23*−*25*). To evaluate the potential nonspecific binding of AMPPNP and AdoMet, the effect of concentration on the observed interproton NOEs was studied. For AMPPNP, one-dimensional TRNOESY experiments were performed as a function of AMPPNP concentration by diluting the sample from a AMPPNP concentration of 10.0 mM to concentrations of 8.0, 6.0, 4.0, and 2.0 mM while keeping the ligand to enzyme concentration ratio fixed at a value of 37:1. The H1′ proton was selectively irradiated in each experiment, and the measurements were done at a single mixing time of 120 ms. The percentage NOE of the H1′−H8 and H1′−H3′ proton pairs was then monitored as a function of AMPPNP concentration since these values should be sensitive to conformational variations. The data indicated that a 10 mM concentration of AMPPNP gave saturation of the active site without adventitious ligand binding. Two-dimensional TRNOESY experiments were then performed on two samples: one containing 4 mM AMPPNP, 0.10 mM AdoMet synthetase, and 8 mM $MgCl_2$ and the second 10 mM AMPPNP, 0.24 mM AdoMet synthetase, and 20 mM $MgCl_2$, as shown in Figure 2. Off-diagonal peaks were not observed in control experiments performed under the same conditions without protein, indicating that cross-peaks reflect cross-relaxation of the bound form of AMPPNP only. NOE build-up curves were obtained by measuring the volumes of the NOE cross-peaks from the data sets at different mixing times (Figure 4) and fitting them as a function of their mixing time using the NOE build-up module of the program FELIX 95. A linear increase in the cross-peak resonance intensity with increasing mixing time indicated that the cross-relaxation rates measured from the initial slope of the NOE build-up curves could be used to extract interproton distances using eq 1. A lag phase prior to the time-dependent increase in peak volume suggested indirect magnetization transfer and indicated that the

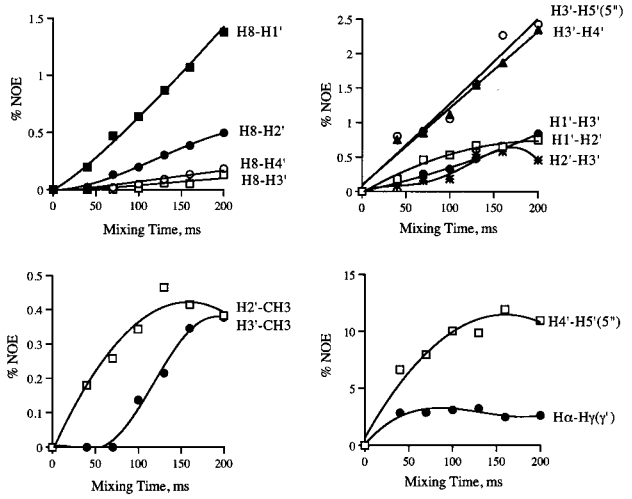

FIGURE 5: NOE intensity build-up curves for the NOE cross-peaks of different proton pairs of AdoMet synthetase-bound AdoMet. The relative NOE intensity of each proton pair was measured as the ratio of the peak volume at different mixing times to the volume of the H1′ diagonal peak at zero mixing time. The volume at zero mixing time of the H1′ diagonal peak was determined by extrapolating the linearly increasing peak volume with decreasing mixing times to zero mixing time.

interproton distance was greater than 4 Å. In this case, cross-relaxation rates were not used to calculate an internuclear distance. The TRNOESY-derived distances obtained were indistinguishable for the two samples, confirming that no adventitious nucleotide binding occurs at 10 mM.

The potential nonspecific binding of (−)-AdoMet to AdoMet synthetase was measured by 1D TRNOESY experiments as described above for AMPPNP. The initial sample containing 8.7 mM AdoMet, 0.28 mM AdoMet synthetase active sites, and 20 mM $MgCl_2$ was successively diluted to 7.0, 5.0, 3.5, and 2.0 mM (−)-AdoMet, keeping the ligand to enzyme concentration ratio constant at a value of 30:1. The percentage NOE of the proton pairs H1′−H8 and H1′−H3′ as a function of AdoMet concentration indicated that a 5 mM (−)-AdoMet concentration assured saturation of the ligand binding site and no adventitious ligand binding was seen up to 8.7 mM. Two-dimensional TRNOESY experiments were then conducted on a sample containing 8.7 mM (−)-AdoMet, 0.28 mM AdoMet synthetase, and 20 mM $MgCl_2$ and on a diluted sample containing 5 mM (−)-AdoMet, 0.16 mM AdoMet synthetase, and 12 mM $MgCl_2$ as shown for a 200 ms mixing time in Figure 3. NOE build-up curves for both experiments were obtained by measuring the volumes of NOE cross-peaks as a function of mixing time according to the procedure described above for AMPPNP. Interproton distances extracted from the initial slope of the NOE build-up curves were indistinguishable for the two experiments, indicating that the data reflect the same AdoMet conformation, thus confirming that no adventitious binding occurs at 8.7 mM AdoMet. Build-up curves for the 8.7 mM AdoMet sample are shown in Figure 5.

The NOE build-up rate of the spatially fixed H1′−H2′ proton pair allows calculation of rotational correlation times of 40 ns for the enzyme·AMPPNP complex and 25 ns for the enzyme·AdoMet complex (*23*−*25*). These correlation times are slightly shorter than the value of 85 ns estimated by Stokes law for a spherical 168 kDa protein, in common with observations in transferred NOESY experiments with other proteins; this difference has typically been attributed to magnetization transfer to protein protons (*23*−*25*). The calculated interproton distances are not sensitive to the correlation time as long as the same correlation time applies to the entire ligand molecule.

Table 1: NOE Build-up Parameters of AMPPNP Bound to AdoMet Synthetase

proton pair	$R_{H1'-H2'}/R_{A-B}$	r_{noe} Å	r_{em} (Å)
H8−H1′	lag phase	>4.0	3.89
H8−H2′	0.637	2.69	3.04
H8−H3′	1.674	3.16	3.53
H8−H4′	lag phase	>4.0	4.79
H8−H5′(5″)	3.198	3.52	3.89, 5.06
H1′-H2′	1.000	2.90	2.99
H1′-H3′	5.560	3.86	3.88
H1′-H4′	1.805	3.20	2.62
H1′-H5′(5″)	lag phase	>4.0	4.60, 4.82
H2′-H3′	0.666	2.71	2.33
H2′-H4′	lag phase	>4.0	3.87
H2′-H5′(5″)	lag phase	>4.0	4.33, 4.98
H3′-H4′	0.827	2.81	3.03
H3′-H5′(5″)	0.696	2.73	2.41, 2.98
H4′-H5′(5″)	0.196	2.21	2.45, 3.06

[a] R_{A-B}, cross-relaxation rate between protons A and B; $R_{H1'-H2'}$, cross-relaxation rate of the H1′−H2′ proton pair; r_{noe}, interproton distance determined from the relative NOE intensity referenced to the H1′−H2′ distance of 2.90 Å; and r_{em}, interproton distance determined from the energy-minimized model. The value of $R_{H1'-H2'}$ was 0.09 s^{-1}. Cross-relaxation rates for the indicated proton pairs are shown as ratios of the rates observed for the H1′−H2′ proton pair to the observed rates of the indicated proton pairs. Cross-relaxation rates were determined from the initial slopes of the NOE build-up curves. R_{noe} values for the H5′(5″) protons reflect an r^6 weighted average of the positions of the two protons. The r_{em} values are for the lowest energy conformer of the family shown in Figure 6.

Conformation of AMPPNP. NOE cross-peaks were seen between proton H8 and the protons in the sugar ring H1′, H2′, H3′, H4′, and H5′(5″) whereas no NOE cross-peaks were observed between proton H2 and the ribose protons. Interproton distances indicated that proton H8 is 2.69 Å apart from the ribose proton H2′ and 3.16 and 3.52 Å away from the ribose protons H3′ and H5′(5″), respectively. Due to the overlap of the resonances of H5′ and H5″, in all analyses signals involving both the H5′ and H5″ protons and a third proton were treated together, and the calculated cross-relaxation rates involving these protons were divided by a factor of 2. The calculated interproton distance of the H8−H5′(5″) proton pair is, therefore, an average distance and does not directly represent the distance of the H8 proton from either the H5′ or the H5″ protons. However, this averaged distance must approximate the correct distance and was therefore used as constraint. A lag phase in the TRNOE build-up curves of the proton pairs H8−H1′ and H8−H4′ indicates that the distance between the two proton pairs is greater than 4 Å. All these distances can be achieved only if AMPPNP adopts an *anti* conformation about its glycosyl bond.

NOE cross-peaks were also observed between the various ribose protons. Interproton distance calculations from the NOE build-up curves indicated that proton H1′ is close to the ribose protons H3′ and H4′ (3.86 and 3.2 Å, respectively), as well as being assigned to a distance of 2.9 Å to H2′ (see Table 1). Proton H3′ is 2.71, 2.73, and 2.81 Å away from protons H2′, H5′(5″), and H4′, respectively. In addition, proton H4′ was found to be in very close proximity (2.21

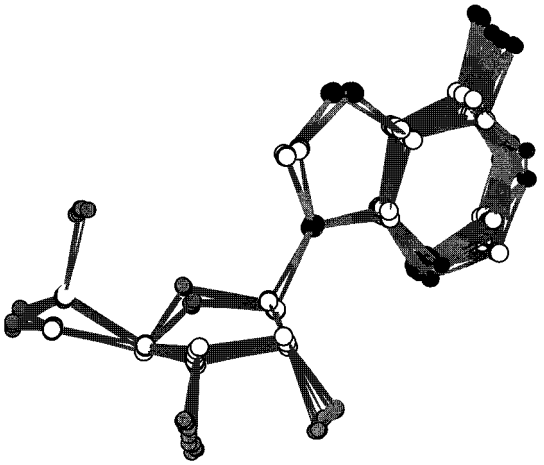

FIGURE 6: Family of computed conformations of the adenosyl moiety of AMPPNP consistent with the NOE constrained distances in Table 1. White, gray, and black circles represent carbon, oxygen, and nitrogen atoms, respectively. Hydrogens have been omitted for clarity.

Table 2: Torsion Angles and Pseudorotation Phase Angle (p) for the Ribose Moiety of the Minimized Model of AMPPNP Bound to AdoMet Synthetase[a]

torsion	angle (deg)	range (deg)
χ(C8−N9−C1′−O4′)	40	39−51
ν_0 (C4′−O4′−C1′−C2′)	−35	−8 to −37
ν_1 (O4′−C1′−C2′−C3′)	12	−9 to −16
ν_2 (C1′−C2′−C3′−C4′)	13	3−23
ν_3 (C2′−C3′−C4′−O4′)	34	−12 to −39
ν_4 (C3′−C4′−O4′−C1′)	43	18−45

$$p = \tan^{-1}\frac{(\nu_4 + \nu_1) - (\nu_3 + \nu_0)}{2\nu_2(\sin 36° + \sin 72°)} = 72$$

[a] The values listed are for the lowest energy conformer. The range of angles reflects those in the family shown in Figure 6.

Å) to protons H5′(5″). The calculated H3′−H5′(5″) and H4′−H5′(5″) distances are average distances as for H8−H5′(5″). Lag phases in the build-up curves of the H1′−H5′(5″), H2′−H5′(5″), and H2′−H4′ proton pairs indicated that these three proton pairs were more than 4 Å apart. Because of the lack of nonexchangeable protons in the PPNP segment of AMPPNP, structural information concerning this part of the molecule was not available.

A constrained energy-minimized model was built based on the NOE-derived interproton distances. Figure 6 shows a superposition of conformations consistent with the NOE constraints. Two possible orientations of the 5′-hydroxyl group are evident, which results from treatment of the H5′, H5″ protons together. The interproton distances of the energy-minimized model (r_{em}) are within a 14% error range of the NOE-derived distances (r_{noe}) (Table 1). As expected, the adenosine ring is in an *anti* conformation with a torsional angle about the glycosyl bond (C8−N9−C1′−O4′) of approximately 40°. The sugar ring moiety is in a $C_{4'}$-*exo* conformation with a pseudorotational phase angle of 72° and a dihedral angle for C1′−C2′−C3′−C4′ of approximately 13°. The torsional angles for the ribose ring in the minimized model are shown in Table 2.

Conformation of AdoMet. In TRNOESY spectra for AdoMet, no NOE cross-peaks were observed between the adenosine proton H2 and the ribose protons of AdoMet, whereas proton H8 showed clear cross-peaks with protons H1′, H2′, H3′, and H4′ of the ribose ring. NOE build-up curves of the various H8−ribose proton pairs showed a linear increase for the H8−H1′ proton pair only. Lag phases were observed in the TRNOE build-up curves of the other H8−ribose proton pairs, indicating that proton H8 is more than 4.0 Å away from the those protons. The interproton distance for the H8−H1′ proton pair was calculated from the initial slope of the NOE build-up curve, giving a distance between the two protons of 2.73 Å. No NOE cross-peaks were observed between proton H8 and the H5′(5″) ribose protons.

NOE cross-peaks were also observed between the ribose protons H1′−H2′, H1′−H3′, H2′−H3′, H3′−H4′, H3′−H5′(5″), and H4′−H5′(5″). Interproton distances calculated from the initial slope of the NOE build-up curves indicated that proton H1′, assigned to 2.90 Å from H2′, is 3.09 Å away from ribose proton H3′. Proton H3′ was found to be very close to proton H4′ (2.41 Å) and 3.02 Å away from proton H2′. In AdoMet, the resonances of the H5′ and H5″ ribose protons overlap, and the cross-relaxation rates involving these protons were divided by a factor of 2, yielding an average distance between these two protons and a third proton. The internuclear distance calculated for the H3′−H5′(5″) proton pairs was 2.73 Å. An average internuclear distance was also calculated between the H4′ and the H5′(5″) protons and was found to be very short (1.85 Å).

The methylsulfonium protons (CH_3) of the methionine moiety of (−)-AdoMet showed NOE cross-peaks with the ribose protons H2′ and H3′. No NOE cross-peaks were seen for the CH_3 protons of (+)-AdoMet. The three protons of the methylsulfonium group of (−)-AdoMet are magnetically equivalent, and the calculated cross-relaxation rates involving these protons were therefore divided by a factor of 3 to give average interproton distances. The average internuclear distance calculated for H2′−CH_3 is 3.37 Å. A lag phase in the NOE build-up curve of the H3′−CH_3 proton pair indicated a separation of more than 4.0 Å. No NOE cross-peaks were observed between the adenosine protons and either the Hα, Hβ(β′), or Hγ(γ′) protons of the methionine moiety, indicating that the methionine group must be oriented away from the adenosine moiety. However, as expected, strong cross-peaks were observed between the Hα−Hβ(β′) and Hβ(β′)−Hγ(γ′) proton pairs of the adjacent groups. Strong cross-peaks were also observed between the Hα and Hγ(γ′) methionine protons. Due to the resonance overlap of protons Hγ and Hγ′, the cross-relaxation rate between these protons was treated like the cross-relaxation rates involving the H5′ and H5″ ribose protons. Interproton distance calculations then indicated that the Hα and Hγ(γ′) protons are as close as 1.90 Å apart.

The constrained energy-minimized model obtained based on the NOE-derived interproton distances showed that the adenosine moiety of AdoMet is in an *anti* conformation about the glycosyl bond with a torsional angle of approximately −27°. The sugar ring is in a $C_{3'}$-*exo* conformation with a pseudorotational phase angle of 214° and a dihedral angle for C1′−C2′−C3′−C4′ of −33°. An interesting difference in the sugar conformations of AMPPNP and AdoMet is the decrease in the H4′−H5′(5″) distance in AdoMet. This change reflects the umbrella-like inversion of configuration at C5′ when the sulfur of methionine displaces the 5′-oxygen

Table 3: NOE Build-Up Parameters of (−)-AdoMet Bound to AdoMet Synthetase

proton pair	$R_{H1'-H2'}/R_{A-B}$	r_{noe} (Å)	r_{em} (Å)
H8−H1′	0.696	2.73	3.19
H8−H2′	lag phase	>4.0	4.09
H8−H3′	lag phase	>4.0	5.54
H8−H4′	lag phase	>4.0	4.40
H1′−H2′	1.000	2.90	2.99
H1′−H3′	1.463	3.09	3.71
H2′−H3′	1.275	3.02	2.51
H3′−H4′	0.329	2.41	2.72
H3′−H5′(5″)	0.696	2.73	2.12, 3.34
H4′−H5′(5″)	0.067	1.85	2.16, 2.72
H2′−CH_3	2.46	3.37	2.84, 3.62, 4.46
H3′−CH_3	lag phase	>4.0	3.83, 4.18, 5.20
Hα−Hγ(γ′)	0.079	1.90	1.90, 3.08

[a] R_{A-B}, cross-relaxation rate between protons A and B; $R_{H1'-H2'}$, cross-relaxation rate of the H1′−H2′ proton pair; r_{noe}, interproton distance determined from the relative NOE intensity referenced to the H1′−H2′ distance of 2.90 Å; and r_{em}, interproton distance determined from the energy-minimized model. The value of $R_{H1'-H2'}$ was 0.06 s^{-1}. Cross-relaxation rates for the indicated proton pairs are shown as ratios of the rates observed for the H1′−H2′ proton pair to the observed rates of the indicated proton pairs. Cross-relaxation rates were determined from the initial slopes of the NOE build-up curves. r_{noe} values for the proton pairs involving the H5′(5″), CH_3, and Hγ(γ′) protons reflect an r^6 weighted average of their positions. The r_{em} values are those of the lowest energy member of the family shown in Figure 7.

Table 4: Torsion Angles and Pseudorotation Phase Angle (*p*) for the Ribose Moiety of the Minimized Model of (−)-AdoMet Bound to AdoMet Synthetase[a]

torsion	angle (deg)	range (deg)
χ(C8−N9−C1′−O4′)	−27	−27 to −33
ν_0(C4′−O4′−C1′−C2′)	−33	−20 to −33
ν_1(O4′−C1′−C2′−C3′)	40	39−43
ν_2(C1′−C2′−C3′−C4′)	−33	−32 to −39
ν_3(C2′−C3′−C4′−O4′)	15	13−28
ν_4(C3′−C4′−O4′−C1′)	11	−2−13

$$p = \tan^{-1}\frac{(\nu_4 + \nu_1) - (\nu_3 + \nu_0)}{2\nu_2(\sin 36° + \sin 72°)} = 214$$

[a] Since ν_2 is negative, 180° was added to the calculated value of *p* (*61*). The angles listed are those of the lowest energy conformer. The range of angles reflects those in the family shown in Figure 7.

of AMPPNP during AdoMet formation. The methylsulfonium group is oriented toward the ribose ring, resulting in NOE signals between the CH_3 protons and the H2′ ribose proton. The NOE-derived distances (r_{noe}) and the distances derived from the energy-minimized model (r_{em}) are shown in Table 3. The r_{noe} and r_{em} generally agree quite well, with the largest variation for interactions where two methylene protons were treated together. The torsional angles for the ribose ring in the minimized model are shown in Table 4. A family of computed conformations consistent with the data are illustrated in Figure 7.

Interaction of AMPPNP with Active Site Amino Acid Residues. The NOE-derived conformation of AMPPNP was docked into the active site of the AdoMet synthetase·ADP·P_i crystal structure, initially by superimposing the adenine base ring of AMPPNP and ADP, and subsequently by positioning the α- and γ-phosphate groups of AMPPNP on the α-phosphate group of ADP and P_i, respectively. The AdoMet synthetase·AMPPNP model obtained was not energy-minimized as the overall conformation adopted by

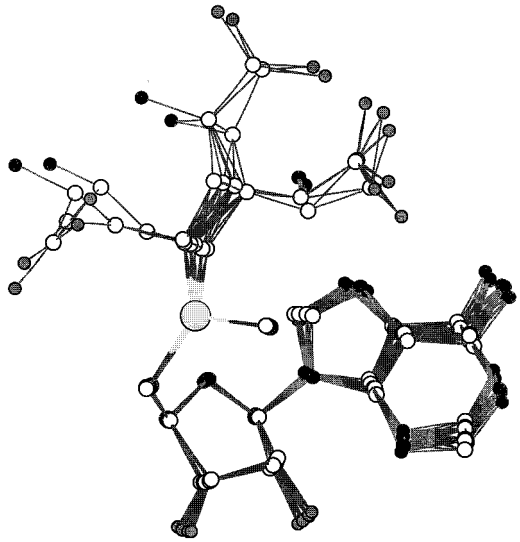

FIGURE 7: Family of computed conformations of AdoMet consistent with the NOE constrained distances in Table 3. White, light gray, dark gray, and black circles represent carbon, sulfur, oxygen, and nitrogen atoms, respectively. Hydrogens have been omitted for clarity.

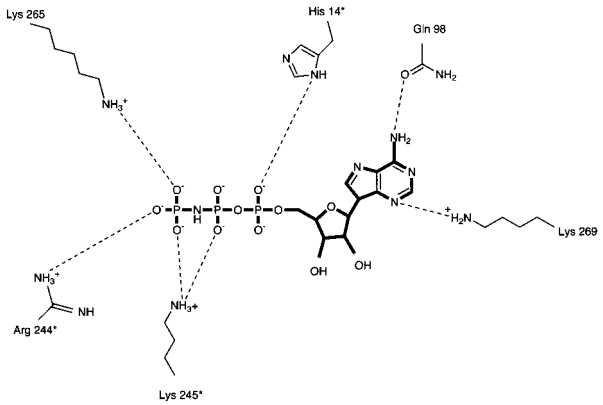

FIGURE 8: Schematic representation of the modeled AdoMet synthetase·AMPPNP complex. The NMR-derived conformation of AMPPNP was docked into the X-ray structure of AdoMet synthetase. Only the residues interacting with AMPPNP are illustrated. The two Mg^{2+} ions are omitted due to uncertainty as to their locations. An asterisk indicates that residues come from a different subunit.

AMPPNP was very similar to that of ADP found in the crystal structure, with the difference that the ribose ring was disordered in the crystal structure and no conformational information was available. Such an approach has been shown to be a valid method for obtaining structural information for a ligand−protein complex (*48*). Figure 8 depicts the model of the AdoMet synthetase·AMPPNP complex thus generated.

AMPPNP lies in the active site pocket with the adenosine ring moiety being located at the entrance of the active site and the tripolyphosphate segment pointing inside the active site cleft. AMPPNP can make roughly the same interactions with the active site amino acid residues and the Mg^{2+} ions that ADP and P_i did in the AdoMet synthetase·ADP·P_i·$2Mg^{2+}$ crystal structure. Like ADP, the AMPPNP adenine base moiety has only two hydrogen bonds to the protein: those being between adenine N3 and Lys 269, and between the adenine N6 amino group and the carbonyl oxygen atom of Gln 98. The importance of the interaction with N6 is consistent with our finding that inosine triphosphate is not a

substrate (<0.1% of the activity of ATP) and at best a weak inhibitor (K_i > 10 mM or >100-fold greater than the K_m for ATP). No hydrogen bonds between the ribose and the protein are observed. Although the sugar ring of ADP in the crystal structure was found to be disordered, it was suggested that Gly 17 and Asp 118 might participate in hydrogen bonding groups through disordered water molecules (*21*). Similar interactions can be suggested from the AMPPNP model. Functional studies imply interaction with the ribose hydroxyls since 2′-deoxy-ATP is not a substrate and is a poor inhibitor (K_i > 5 mM) while 3′-deoxy-ATP is a good substrate with a K_m of ∼0.1 mM, equivalent to ATP, and a V_{max} of ∼60% of ATP (*9*).

The interaction of the polyphosphate segment of AMPPNP and the protein is of particular interest since it undergoes chemical transformation during catalysis. In the crystal structure of the AdoMet synthetase·ADP·P_i complex, the polyphosphate moiety interacts extensively with the enzyme, and a similar interaction with the polyphosphate moiety of AMPPNP could be modeled. A few differences were, however, noticeable. The γ-phosphate of AMPPNP can occupy the same position as free P_i in the crystal structure. One γ-phosphate oxygen points toward Lys 265 and may also interact with Arg 244* (the active site lies between two subunits, and the asterisk indicates that the residue comes from a second subunit), consistent with results of mutagenesis studies (Figure 8) (*49*). A second γ-phosphate oxygen is within hydrogen bonding distance of Lys 245*. An important difference between AMPPNP and ADP was observed in the position and coordination of the β-phosphate group to the protein. The β-phosphate group of AMPPNP is ∼2.6 Å closer to Lys 245* than the β-phosphate of ADP, and a β-phosphate oxygen points toward Lys 245*. A 1 Å movement of the AMPPNP α-phosphate group from the α-phosphate position of ADP was also observed. This brings the α-phosphate group of AMPPNP closer to the position occupied by the β-phosphate group of ADP. The α-phosphate oxygen of AMPPNP is now only ∼3.9 Å away from His 14*. It seems likely that this hydrogen bonding pattern around the tripolyphosphate segment of AMPPNP is responsible for the high affinity of the PPNP generated by reaction of AMPPNP and methionine, so that PPNP dissociates >10^4-fold more slowly than PPi (*9*).

AMPPNP is believed to be structurally almost indistinguishable from ATP (*50*). Therefore, it is likely that the conformation adopted by AMPPNP and the interactions between AMPPNP and the enzyme reflect those adopted by ATP. A slight movement of the α−β-polyphosphate moiety may occur after hydrolysis of the ATP β−γ-polyphosphate bridge and lead to the conformation of ADP found in the crystal structure. Since the two Mg^{2+} ions may alter their position from those occupied in the AdoMet synthetase·ADP·P_i crystal structure, they are not included in the active site schematic. Alternate metal coordination schemes have been observed in other AdoMet synthetase crystal structures such as the enzyme·2P_i·2Mg^{2+} structure (*20*), and variabilities in metal coordination have been inferred by EPR studies of Mn^{2+} complexes (*7*).

Interaction of AdoMet with Amino Acid Residues. The computed conformation of AdoMet was docked in the active site by first superimposing the adenine of AdoMet with that of ADP found in the crystal structure. This maintains the N3 and N6 atoms of the adenine ring of AdoMet within hydrogen bonding distance from Lys 269 and Gln 98, respectively (Figure 9). No interactions between the ribose ring of AdoMet and the protein were observed. The α-carbon carboxyl and amino substituents of AdoMet, for which no NOEs were visible because of the lack of nonexchangeable protons, were then modeled into the enzyme active site. Hydrogen bonds could be found between the amino group and Asp 238. No additional protein−ligand interactions were found for the methionyl moiety; the apparent lack of interactions with the carboxyl group is consistent with the observation that methionine methyl ester is a good substrate with a K_m of 0.5 mM, only 7-fold higher than methionine, and gives 90% of the V_{max} of methionine (*7*).

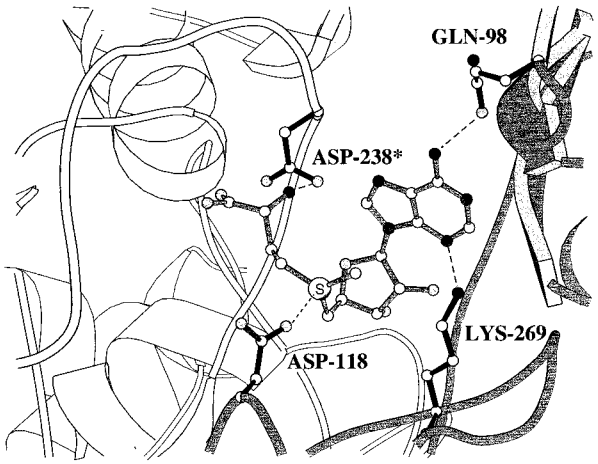

FIGURE 9: Model of the AdoMet synthetase·AdoMet complex. The NMR-derived conformation of AdoMet was docked into the X-ray structure of AdoMet synthetase. Only the residues interacting with AdoMet are shown. An asterisk indicates that residues come from a different subunit. The two subunits that contribute to the active site are shaded differently. This figure was prepared with MolScript (*62*).

Electrostatic interactions between oxygens of peptide bonds, or of Glu or Asp side chains, and the charged S^+ atom of AdoMet have been seen in the crystal structures of several enzyme·AdoMet complexes such as *E. coli* met repressor (*51*), Hhal DNA methyltransferase (*52*), glycine *N*-methyltransferase (*53*), and the adenine-specific DNA methyltransferase M·TaqI (*54*, *55*). A similar interaction can occur between AdoMet synthetase and AdoMet via rotation of the side chain of Asp 118 which could bring an oxygen within van der Waals contact of the sulfur. The NOE-derived conformation of AdoMet also places the sulfur at a van der Waals contact with the ribose O4′. The positive charge of the sulfur appears to be quite important in AdoMet binding since the uncharged *S*-adenosylhomocysteine does not inhibit the enzyme (*9*). The importance of close electrostatic sulfur−oxygen nonbonded interactions in ligand binding has been noted even in systems with formally uncharged sulfur atoms (*56*).

CONCLUSIONS

The NOE-derived conformations of AMPPNP and AdoMet bound to AdoMet synthetase show that both compounds bind with *anti*, but distinct, glycosidic bond angles. The AMPPNP angle of 40° is near the range of 52 ± 8° found for several other adenosine nucleotide utilizing enzymes (*25*). The glycosidic angle for AdoMet of −27° reflects a significant rotation from that in AMPPNP, which may reflect

the larger steric requirements of the trivalent 5′-sulfur substituent in AdoMet than the bivalent oxygen substituent of the polyphosphate chain in nucleotides. A wide range of glycosidic bond angles, encompassing both the *syn* and *anti* regions, have been reported in crystal structures of AdoMet utilizing methyltransferases (*53*−*55*, *57*−*60*). The enzyme's large active site cavity is well suited to accommodate these conformational alterations. The models built by combination of the present NOE data and the protein crystal structure provide new reference points for the design and analysis of numerous site-directed mutants and of novel inhibitors under ongoing investigation.

ACKNOWLEDGMENT

We thank Drs. Y.-Z. Zhang and H. Chen for advice on NMR methodology and assistance in NMR instrument operation.

REFERENCES

1. Tabor, C. W., and Tabor, H. (1984) *Adv. Enzymol. Relat. Areas Mol. Biol. 56*, 251−282.
2. Cantoni, G. L. (1975) *Annu. Rev. Biochem. 44*, 435−451.
3. Kappler, F., and Hampton, A. (1990) *J. Med. Chem. 33*, 2545−2551.
4. Sufrin, J. R., Lombardini, J. B., and Alks, V. (1993) *Biochim. Biophys. Acta 1202*, 87−91.
5. Mudd, S. H., and Cantoni, G. L. (1958) *J. Biol. Chem. 231*, 481−492.
6. Cantoni, G. L. (1953) *J. Biol. Chem. 204*, 403−416.
7. Markham, G. D. (1981) *J. Biol. Chem. 256*, 1903−1909.
8. Zhang, C., Markham, G. D., and Lobrutto, R. (1993) *Biochemistry 32*, 9866−9873.
9. Markham, G. D., Hafner, E. W., Tabor, C. W., and Tabor, H. (1980) *J. Biol. Chem. 255*, 9082−9092.
10. Markham, G. D., DeParasis, J., and Gatmaitan, J. (1984) *J. Biol. Chem. 259*, 14505−14507.
11. Thomas, D., and Surdin-Kerjan, Y. (1987) *J. Biol. Chem. 262*, 16704−16709.
12. Thomas, D., Rothstein, R., Rosenberg, N., and Surdin-Kerjan, Y. (1988) *Mol. Cell. Biol. 8*, 5132−5139.
13. Peleman, J., Saito, K., Cottyn, B., Engler, G., Seurinck, J., Van Montagn, M., and Inze, D. (1989) *Gene (Amsterdam) 84*, 359−369.
14. Peleman, J., Boerjan, W., Engler, G., Seurinck, J., Botterman, J., Alliote, T., Van Montegu, M., and Inze, D. (1989) *Plant Cell 1*, 81−93.
15. Horikawa, S., Sasuga, J., Shimuzu, K., Ozasa, H., and Tsukada, K. (1990) *J. Biol Chem. 265*, 13683−13686.
16. Horikawa, S., and Tsukada, K. (1991) *Biochem. Int. 25*, 81−90.
17. Horikawa, S., and Tsukada, K. (1993) *FEBS Lett. 312*, 37−41.
18. Larsen, P. B., and Woodson, W. R. (1991) *Plant Physiol. 96*, 997−999.
19. Horikawa, S., Ishikawa, M., Ozasa, H., and Tsukada, K. (1989) *Eur. J. Biochem. 184*, 497−501.
20. Takusagawa, F., Kamitori, S., Misaki, S., and Markham, G. D. (1996) *J. Biol. Chem. 271*, 136−147.
21. Takusagawa, F., Kamitori, S., and Markham, G. D. (1996) *Biochemistry 35*, 2586−2596.
22. Plesniak, L. A., Yu, L., and Dennis, E. A. (1995) *Biochemistry 34*, 4943−4951.
23. Jarori, G. K., Murali, N., and Nageswara Rao, B. D. (1994) *Biochemistry 33*, 6784−6791.
24. Murali, N., Jarori, G. K., Landy, S. B., and Nageswara Rao, B. D. (1993) *Biochemistry 32*, 12941−12948.
25. Murali, N., Lin, Y., Mechulam, Y., Plateau, P., and Nageswara Rao, B. D. (1997) *Biophys. J. 70*, 2275−2284.
26. Song, S., Velde, D. V., Gunn, C. W., and Himes, R. H. (1994) *Biochemistry 33*, 693−698.
27. Stewart, J. M. M., Jorgensen, P. L., and Grisham, C. M. (1989) *Biochemistry 28*, 4695−4701.
28. Rosevear, P. R., Bramson, H. N., O′Brian, C., Kaiser, E. T., and Mildvan, A. S. (1983) *Biochemistry 22*, 3439−3447.
29. Perlman, M. E., Davis, D. G., Koszalka, G. W., Tuttle, J. V., and London, R. E. (1994) *Biochemistry 33*, 7547−7559.
30. Koblan, K. S., Culberson, J. C., Desolms, S. J., Giuliani, E. A., Mosser, S. D., Omer, C. A., Pitzenberger, S. M., and Bogusky, M. J. (1995) *Protein Sci. 4*, 681−688.
31. Ehrlich, R. S., and Colman, R. F. (1990) *Biochemistry 29*, 5179−5187.
32. Seelig, G. F., Prosise, W. W., Hawkins, J. C., and Senior, M. M. (1995) *J. Biol. Chem. 270*, 9241−9249.
33. Schalk-Hihi, C., Zhang, Y.-Z., and Markham, G. D. (1998) *Biochemistry 37*, 7608−7616.
34. Sanders, C. R., II, and Tsai, M.-D. (1988) *J. Am. Chem. Soc. 110*, 3323−3324.
35. Park, J., Tai, J., Roessner, C. A., and Scott, A. I. (1996) *Bioorg. Med. Chem. 5*, 2179−2185.
36. Cutnell, J. D., Dallas, J., Matson, G., LaMar, G. N., Rink, H., and Rist, G. (1980) *J. Magn. Reson. 41*, 213−221.
37. Chylla, R. A., and Markley, J. L. (1993) *J. Magn. Reson. 102*, 148−154.
38. DeLeeuw, H. P. M., Haasnoot, L. A., and Altona, C. (1980) *Isr. J. Chem. 20*, 108.
39. Lewitt, M., and Warshel, A. (1978) *J. Am. Chem. Soc. 100*, 2607−2613.
40. Scott, K., Stonehouse, J., Keeler, J., Hwang, T.-L., and Shaka, A. J. (1995) *J. Am. Chem. Soc. 117*, 4199−4200.
41. Stonethouse, J., Adell, P., Keeler, J., and Shaka, A. J. (1994) *J. Am. Chem. Soc. 116*, 6037−6038.
42. Scott, K., Keller, J., Van, Q. N., and Shaka, A. J. (1997) *J. Magn. Reson. 125*, 302−324.
43. Sack, J. S. (1988) *J. Mol. Graph. 6*, 224−225.
44. André, F., Demassier, V., Bloch, G., and Neumann, J.-M. (1990) *J. Am. Chem. Soc. 112*, 6784−6789.
45. Beaudouin, C., Haurta, G., Laffitte J. A., and Renaud, B. (1993) *J. Neurochem. 61*, 928−935.
46. Stolowitz, M. L., and Minch, M. J. (1981) *J. Am. Chem. Soc. 103*, 6015−6019.
47. Hoffman, J. L. (1986) *Biochemistry 25*, 4444−4449.
48. Gradwell, M. J., and Feeney, J. (1996) *J. Biomol. NMR 7*, 48−58.
49. Reczkowski, R. S., Taylor, J. C., and Markham, G. D. (1998) *Biochemistry 38*, 13499−13506.
50. Taylor, J. S. (1981) *J. Biol. Chem. 256*, 9793−9795.
51. Rafferty, J. B., Somers, W. S., Saint-Girons, I., and Phillips, S. E. V. (1989) *Nature 341*, 705−710.
52. Cheng, X., Kumar, S., Posfai, J., Pflugrath, J. W., and Roberts, R. J. (1993) *Cell 74*, 299−307.
53. Fu, Z., Hu, Y., Konishi, K., Takata, Y., Ogawa, H., Gomi, T., Fujioka, M., and Takusagawa, F. (1996) *Biochemistry 35*, 11985−11993.
54. Schluckebier, G., Kozak, M., Bleimling, N., Weinhold, E., and Saenger, W. (1997) *J. Mol. Biol. 265*, 56−67.
55. Labahn, J., Granzin, J., Schluckebier, G., Robinson, D. P., Jack, W. E., and Schildkraut, I. (1994) *Proc. Natl. Acad. Sci. U.S.A. 91*, 10957−10961.
56. Li, H., Hallows, W. H., Punzi, J. S., Marquez, V. E., Carrell, H. L., Pankiewicz, K. W., Watanabe, K. A., and Goldstein, B. M. (1994) *Biochemistry 33*, 23−32.
57. Gong, W., O'Gara, M., Blumenthal, R. M., and Cheng, X. (1997) *Nucleic Acids Res. 25*, 2702−2715.
58. Hodel, A. E., Gershon, P. D., Shi, X., and Quiocho, F. A. (1996) *Cell 85*, 247−256.
59. Dixon, M. M., Huang, S., Matthews, R. G., and Ludwig, M. (1996) *Structure 4*, 1263−1275.
60. O'Gara, M., Roberts, R. J., and Cheng, X. (1996) *J. Mol. Biol. 263*, 597−606.
61. Altona, C., and Sundaralingam, M. (1972) *J. Am. Chem. Soc. 94*, 8205−8212.
62. Kraulis, P. J. (1991) *J. Appl. Crystallog. 24*, 946−950.

BI9822933